Indian Journal of Pure & Applied Physics
Vol. 60, June 2022, pp. 497-508

Temperature and Mass Dispersion of Free Convective Radiative Non - Newtonian Nano Fluid Flow between Two Parallel Plates

R Arpitha & D Srikanth*

Department of Applied Mathematics, Defence Institute of Advanced Technology (Deemed to be University), Pune – 411 025, India

Received 7 March 2022; accepted 17 May 2022

In the current study, impact of the thermal radiation along with thermophoretic diffusion and Brownian motion ramifications on the flow of non-Newtonian nanofluid represented by Couple stress fluid between horizontal parallel plates are discussed. Where the parallel plates are kept at various temperatures and concentrations, the fluid is periodically sucked and injected at the upper plate and lower plate respectively. The governing non-linear partial differential equations are reduced into a non-linear system of ordinary differential equations with the aid of similarity transformations. The resultant non-dimensional equations are subsequently solved by using shooting-method with the usual 4th order Runge-Kutta scheme. The non-dimensional velocity and temperature variations along with mass transfer profiles are analyzed for different fluid and parameters as well as geometric parameters and the same are plotted in the form of graphs. Skin- friction coefficient in non-dimensional along with heat & mass transfer rates are studied numerically. It is found that there is a direct relationship between temperature component of the fluid and the Brownian movement parameter, while the concentration component of the fluid is decreasing with respect to that of thermophoresis parameter. Further, mass transfer decreases with increasing couple stress fluid parameter.

Keywords: Couple stress nanofluid; Brownian motion; Thermophoresis; Shooting method; Thermal radiation

1 Introduction

In the last few decades, significant number of researchers across the globe have focused on the problems related to the flow of the non-Newtonian fluids, as it has vast applications in industries such as slurry transport, petroleum industry, polymeric liquids, glass fiber, shampoos, paints, soaps, tomato paste, paper production, etc. In order to examine the non-Newtonian behavior of fluids, scientists have developed distinct models. One such fluid model is due to the couple stress fluid. This model was initially established by Stokes in 1960[1]. The same author reported a detailed review in 1984[2], which included some exact solutions to the classical flow problems such as Poiseuille, Couette, and Hagen-Poiseuille flow, etc. Srinivasacharya *et al.*[3] described in detail the flow of the couple stress fluid in a slit that is permeable. Devakar & Iyengar[4] developed an analytical solution for an incompressible run-up flow of the couple stress fluid in a channel conduit. The impact of a dependent heat source on magnetohydrodynamics, on the mixed convective flow of that of couple stress fluid with the assumption of Hall currents and Ion-slip currents was discussed by Srinivasacharya and Kaladhar[5]. Aksoy[6] scrutinized the impact of heat flux over entropy of flow of that of the couple stress fluid confined to the middle of two plates which are parallel. Ojjela & Kumar[7] have discovered the impact of Soret and Dufour impacts on MHD (magnetohydrodynamics) incompressible flow of the radiative non-Newtonian couple stress fluid by considering mixed convection and also the chemical reaction in a channel. Hayat *et al.*[8] described the squeezing flow of the MHD couple stress nanofluid along with the plates that are parallel. Subsequently, many researchers have focused on the study of considering the flow related to non-Newtonian fluids along the porous boundaries with suction/injection because of their vast applications in science and technology. Real-life uses of some of these are soil absorption, preservation of food, transportation of groundwater-related to petroleum industries, blood flow in the arteries, aerodynamics heating, polymer technology, artificial dialysis *etc*., Various such studies have been listed in the form of references[9-14].

Fluid flow which is caused by density differences and is associated with temperature and concentration changes due to cooling or heating effect is known as free or natural convection. Natural convection has significant applications in geology, energy storage

*Corresponding author: (E-mail: sri_dasari1977@yahoo.co.in)

devices, solar receiver systems, *etc*., Nakamura *et al.*[15] explored the heat transfer profiles of the natural convective flow of Newtonian fluid between two infinite parallel plates. Narahari[16] studied the natural convective radiative Couette flow of a viscous fluid in the middle of two vertical plates which are parallel to each other. Narahari & Dutta[17] examined the heat transfer in a free convective flow of a Newtonian fluid in a vertical channel. Jha & Ajibade[18] considered the flow of free convection with a periodic temperature regime at the boundaries. Jha & Aina[19] highlighted the flow of free convective of an MHD Newtonian fluid in a vertical microchannel.

Among all the modes of heat transfer, radiation is a different form of heat transfer mode and it does not need any medium for its transmission. Whenever two objects having different temperatures are placed at a finite distance apart, the net energy will be transferred from an object having higher temperature to the lower temperature object. In real life, we can see the radiation in the form of the sun transmitting heat to the earth. Alagoa *et al.*[20], have analyzed the radiation effects on the MHD convective fluid flow along with the porous medium which is confined between infinite parallel plates. Kumar *et al.*[21], discussed the non-linear thermal radiation effect on electrically conducting fluid flow in a narrow channel, wherein they have assumed that the thermal radiation parameter is directly proportional to the temperature profiles. Dogonchi *et al.*[22], in their paper modeled the Newtonian nanofluid squeezing flow between the infinite parallel plates under the thermal radiation effect. Hassan *et al.*[23], analyzed the radiative heat impact on MHD (magnetohydrodynamics) flow of a reactive hydromagnetic fluid confined between parallel porous plates. Reddy *et al.*[24], described heat as well as mass characteristics of an MHD nanofluid with thermal radiation impacts over an inclined flat plate and concluded that, heat and mass characteristics increase with an increase in magnetic field parameter. Sandhya *et al.*[25], in their study observed that the velocity, temperature and concentration fields decrease with increasing values of radiation parameter. The randomly motion of the suspended particles in the fluid due to their collisions with the surrounding gaseous molecules is termed Brownian motion. For the small particles that scatter both in hotter and colder regions, the velocity of the particles is higher in hotter regions compared to that of colder regions, as a result of which the particles collide and move towards the colder region. The force that pushes them is known as thermophoretic force. Firstly, this effect was discovered by Brown[26], later this was studied in "Convective Transport in Nanofluids" by Buongiorno[27]. Guha & Samanta[28] have considered the thermophoresis effect on aerosol particle transport in free convection flow on horizontal plates. Mahmoodi and Kandelousi[29] have analyzed the entropy generation, thermophoretic diffusion, and Brownian motion sway on nanofluid and concluded that Nusselt number has diminished with the enhancement of thermophoretic and Brownian motion parameters. Hayat *et al.*[30] have considered the Brownian movement and also the thermophoretic diffusion over the MHD squeezing nanofluid flow on the stretching surface that is porous. Sheikholeslami *et al.*[31] considered steady nanofluid flow with the thermophoretic diffusion and Brownian motion sway between parallel plates and solved the constitutive relations by means of the differential transformation method. Reddy *et al.*[32] have examined Brownian motion and thermophoresis sway on the flow of an electrically conducting fluid on a slandering stretching surface.

With an inspiration from the above works, we propose to analyze the heat and mass characteristics in the natural convective flow of a couple-stress nanofluid along a porous medium confined to the middle of parallel plates under the influence of the thermal radiation, thermophoretic diffusion and Brownian movement effects. The dimensionless components of velocity, concentration profile, temperature distribution, the coefficient of skin-friction, mass characteristics rate and heat characteristics rate with reference to diverse geometric parameters and fluid parameters are displayed graphically and also in the form of neat tables.

2 Mathematical description

Considered an unsteady flow of an incompressible non-Newtonian nanofluid represented by the Couple stress fluid. The flow is considered in a porous medium which is confined between two horizontal parallel plates such that the plates are at h distance apart from each other and they position at Y=0 and Y=h as appeared in Fig. 1. Assumed that there is a periodic injection through the lower-plate and a periodic suction through the upper- plate in the form of $V_1 e^{i\omega t}$ and $V_2 e^{i\omega t}$ respectively, with $|V_2| \geq |V_1|$. Concentration and temperatures are considered to be

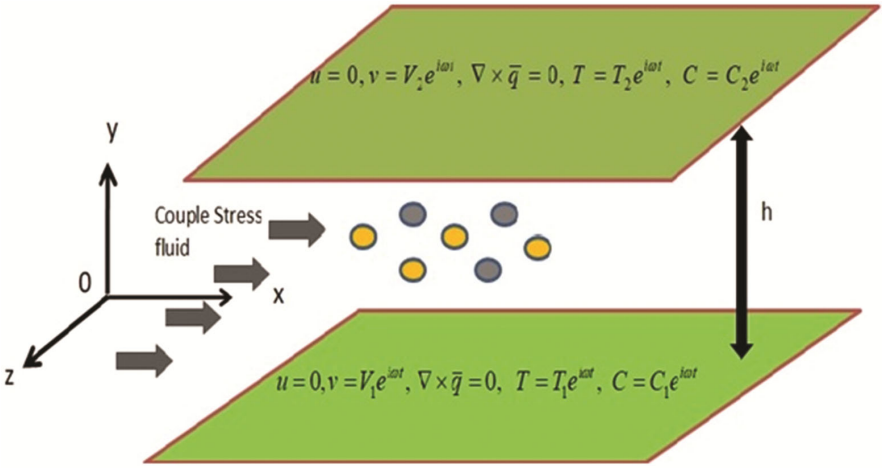

Fig. 1 — Geometry of the fluid flow.

periodic at the boundaries. The *X*-axis and *Y*- axis are chosen, along parallel and in perpendicular direction of the primary flow as specified below in the Fig. 1.

The equations governing the flow of couple stress fluid for energy and concentration under the impact of radiation, thermophoretic diffusion, and Brownian motion parameter in reference frame are as given in[1],

$$\nabla . \bar{q} = 0 \quad \ldots (1)$$

$$\rho\left(\frac{\partial \bar{q}}{\partial t} + \bar{q}(\bar{q}.\nabla)\right) = -\nabla P + \mu\nabla^2\bar{q} - \eta\nabla^4\bar{q} - \frac{\mu}{K_1}\bar{q} + \bar{F}_b \quad \ldots (2)$$

$$\rho c\left(\frac{\partial T}{\partial t} + T(\bar{q}.\nabla)\right) = K\nabla^2\bar{q} + 4\eta(\nabla\bar{\omega}:(\nabla\bar{\omega})') + 4\eta'(\nabla\bar{\omega}:(\nabla\bar{\omega})') + \tau_1(\rho c)\left[(\nabla \mathrm{T}.\nabla \mathrm{C})D_B + (\nabla \mathrm{T}.\nabla \mathrm{T})\frac{D_T}{T_2}\right] - \frac{\partial q_r}{\partial y} + \frac{\mu}{K_1}|q|^2 + 2\mu D:D \quad \ldots (3)$$

$$\left(\frac{\partial C}{\partial t} + C(\bar{q}.\nabla)\right) = D_B\nabla^2 C + \frac{\mathrm{D_T}}{\mathrm{T_2}}\nabla^2 T \quad \ldots (4)$$

Where $\bar{q} = u\hat{\imath} + v\hat{\jmath}$, $\tau_1 = \frac{(\rho C)_p}{(\rho C)_f}$ and buoyancy force $\bar{F}_b = \left[\left(T - T_1 e^{i\omega t}\right)\rho g\beta_T + \left(C - C_1 e^{i\omega t}\right)\rho\beta_C\right]\hat{\jmath}$ ...(5)

The velocity, concentration & temperature transformations are

$$u(x,\lambda,t) = f'(\lambda)e^{i\omega t}\left(-\frac{V_2 x}{h} + \frac{U_0}{a}\right)$$

$$v(x,\lambda,t) = V_2 f(\lambda)e^{i\omega t}$$

$$T(x,\lambda,t) = \left[T_1 + \frac{\mu v_2}{\rho hc}\left(\emptyset_1(\lambda) + \left(\frac{U_0}{av_2} - \frac{x}{h}\right)^2\right)\emptyset_2(\lambda)\right]e^{i\omega t}$$

$$C(x,\lambda,t) = \left[C_1 + \frac{\eta_A}{h\vartheta}\left(g_1(\lambda) + \left(\frac{U_0}{av_2} - \frac{x}{h}\right)^2\right)g_2(\lambda)\right]e^{i\omega t} \quad \ldots (6)$$

Rosseland's approximation for radiative heat flux (q_r) in the energy equation, as given by

$$q_r = -\frac{4\sigma^*}{3K^*}\frac{\partial T^4}{\partial y} \quad \ldots (7)$$

Then by using Taylor's series, T^4 can be expanded as

$$T^4 = T_1^4 + 4T_2^3(T - T_1) + 6T_2^2(T - T_1)^2 + \quad \ldots (8)$$

By omitting the higher degree terms, which are beyond the first degree of $(T - T_1)$ in equation (8), we obtain $T^4 = T_1^4 + 4T_2^3(T - T_1)$ substituting this in equation (7), we get

$$q_r = -\frac{16T_1\sigma^*}{3K^*}\frac{\partial T}{\partial y} \quad \ldots (9)$$

The initial and boundary conditions are taken as follows

$$u = 0, v = v_1 e^{i\omega t}, \nabla \times \bar{q} = 0, T = T_1 e^{i\omega t}, C = C_1 e^{i\omega t} \text{ at } y = 0$$

$$u = 0, v = v_2 e^{i\omega t}, \nabla \times \bar{q} = 0, T = T_2 e^{i\omega t}, C = C_2 e^{i\omega t} \text{ at } y = h \quad \ldots (10)$$

Substituting (6) in (2), (3), and (4) it is seen that

$$f^{vi} = \frac{1}{\alpha^2}[Re(f'f'' - ff''')cos\beta - Da\, f'' + 2Gr\, Ec\, \emptyset_2 + 2Gm\, Sh\, g_2 + f^{iv}] \quad \ldots (11)$$

$$\emptyset_1'' = \frac{1}{(1+Rd)}\left[-\mathrm{Pr}Re\left(4f'^2 + f^2 Da + f''^2\alpha^2 - f\emptyset_1'\right)cos\beta - Nt\, EC\, \emptyset_1'^2 cos\beta - Nb\, Sh\emptyset_1' g_1' cos\beta\right] - 2\,\emptyset_2 \quad \ldots (12)$$

$$\emptyset_2'' = \frac{1}{(1+Rd)}\begin{bmatrix} -\Pr Re\left(f''^2 + f'''^2\alpha^2 + f'^2 Da - f\emptyset_1' + 2f'\emptyset_2\right)cos\beta \\ -Nb\ sh(4\emptyset_2' g_2 + \emptyset_2' g_2' \xi^2 + \emptyset_1' g_2' + \emptyset_2' g_1')\ cos\beta \\ -Nt\ Ec\ \left(2\emptyset_1'\emptyset_2' + 4\emptyset_2^2 + \emptyset_2'^2 \xi^2\right) cos\beta \end{bmatrix} \quad \ldots (13)$$

$$g_1'' = Re\ Sc\ f g_1'\ cos\beta - \frac{Nt\ Ec}{Nb\ sh}(2\emptyset_2 + \emptyset_1'') - 2g_2 \quad \ldots (14)$$

$$g_2'' = Re\ Sc\ (-2f' g_2 + f g_2')cos\beta - \emptyset_2'' \frac{Nt\ Ec}{Nb\ sh} \quad \ldots (15)$$

$f, \emptyset_1, \emptyset_2, g_1\ and\ g_2$ are functions in terms of λ to be computed and the prime in the above equations represent the derivative with respect to λ alone.

The non-dimensional form of concentration distribution and temperature distribution from Eq. (6) are as given below

$$u^* = \xi f' e^{i\omega t}, v^* = f e^{i\omega t}, T^* = \frac{T - T_1 e^{i\omega t}}{(T_2 - T_1)e^{i\omega t}} = Ec(\emptyset_1 + \xi^2 \emptyset_2),$$
$$C^* = \frac{C - C_1 e^{i\omega t}}{(C_2 - C_1)e^{i\omega t}} = Sh(g_1 + \xi^2 g_2)$$

The non dimensional initial and boundary conditions (10) for $f,\ \phi_1\ ,\phi_2, g_1$ and g_2 are

$$f(0) = 1 - a; f(1) = 1, f'(0) = 0, f'(1) = 0, f''(0) = 0, f''(1) = 0, \varphi_1(0) = 0;$$
$$\varphi_1(1) = \frac{1}{Ec}, \varphi_2(0) = 0; \varphi_2(1) = 0, g_1(0) = 0; g_1(1) = \frac{1}{sh}, g_2(0) = 0; g_2(1) = 0 \quad \ldots (16)$$

The non dimensional skin friction coefficient due to couple stress fluid flow is $S_f = \left(\frac{\tau_{xy}}{\rho v_2^2}\right)_{\lambda=0,1}$ where

$$\tau_{xy} = \left(\mu \frac{\partial \mu}{\partial y} - \eta \frac{\partial^3 \mu}{\partial y^3}\right)_{\lambda=0,1} = \frac{2}{Re}\left(\frac{U_0}{av_2} - \frac{x}{h}\right) * \left(f'' - \alpha^2 f^{iv}\right)cos\omega t \quad \ldots (17)$$

The heat transfer rate (Nusselt number) through the lower- plate (λ=0) and the upper-plate (λ=1) are given by

$$Nu = -\frac{(1+Rd)\frac{\partial T}{\partial y}}{\frac{(T_2 - T_1)}{h}} = -(1 + Rd)\left[\emptyset_1'(\lambda) + \left(\frac{U_0}{av_2} - \frac{x}{h}\right)^2 \emptyset_2'(\lambda)\right]_{\lambda=0,1} \quad \ldots (18)$$

The rate of mass transfer (Sherwood number) through the lower- plate (λ=0) and the upper- plate (λ=1) are given by

$$sh = \frac{Mass\ Transfer\ rate}{Diffusion\ rate} = \left[g_1'(\lambda) + \left(\frac{U_0}{av_2} - \frac{x}{h}\right)^2 g_2'(\lambda)\right]_{\lambda=0,1} \quad \ldots (19)$$

3 Numerical Solution of the problem

The non-linear ODEs (12), (13), (14) and (15) are transformed to a system of first order ODEs by the following substitution

$$(f, f', f'', f''', f'^v, f^v, \varphi_1, \varphi_1', \varphi_2, \varphi_2', g_1, g_1', g_2, g_2') = (z_1. z_2, z_3, z_4, z_5. z_6, z_7, z_8, z_9. z_{10}, z_{11}. z_{12}, z_{13}, z_{14},)$$

$$\frac{dz_1}{d\lambda} = z_2, \frac{dz_2}{d\lambda} = z_3, \frac{dz_3}{d\lambda} = z_4, \frac{dz_4}{d\lambda} = z_5, \frac{dz_5}{d\lambda} = z_6$$

$$\frac{dz_6}{d\lambda} = \frac{1}{\alpha^2}[Re(z_2 z_3 - z_1 z_4)cos\beta - Da\ z_3 + 2Gr\ Ec\ z_9 + 2Gm\ Sh\ z_{13} + z_5]$$

$$\frac{dz_7}{d\lambda} = z_8$$

$$\frac{dz_8}{d\lambda} = \frac{1}{(1+Rd)}\begin{bmatrix} -\Pr Re(4{z_2}^2 + {z_1}^2 Da + {z_3}^2\alpha^2 - z_1 z_8)cos\beta \\ -Nt\ EC\ {z_8}^2 cos\beta - Nb\ Shz_8 z_{12}\ cos\beta \end{bmatrix} - 2\ z_9$$

,

$$\frac{dz_9}{d\lambda} = z_{10}$$

$$\frac{dz_{10}}{d\lambda} = \frac{1}{(1+Rd)}\begin{bmatrix} -\Pr Re({z_3}^2 + {z_3}^2\alpha^2 + {z_3}^2 + {z_2}^2 Da - z_1 z_{10} + 2z_2 z_9) \\ -Nb\ sh(4z_9 z_{13} + z_8 z_{14} + z_{10} z_{12} + z_{10} z_{14}\xi^2) \\ -Nt\ Ec\ (2z_8 z_{10} + 4{z_9}^2 + {z_{10}}^2 \xi^2) \end{bmatrix} cos\beta$$

$$\frac{dz_{11}}{d\lambda} = z_{12}$$

$$\frac{dz_{12}}{d\lambda} = Re\ Sc\ z_1 z_{12}\ cos\beta - \frac{Nt\ Ec}{Nb\ sh}\left(2z_9 + \frac{dz_8}{d\lambda}\right) - 2z_{13}$$

$$\frac{dz_{13}}{d\lambda} = z_{14}$$

$$\frac{dz_{14}}{d\lambda} = Re\ Sc\ (-2z_2 z_{13} + z_1 z_{14})cos\beta - \frac{dz_{10}}{d\lambda}\frac{Nt\ Ec}{Nb\ sh} \quad \ldots (20)$$

The initial conditions chosen are as given below

$$z_1(0) = 1 - a, z_2(0) = 0, z_3(0) = 0, z_4(0) = a_1, z_5(0) = a_2, z_6(0) = a_3, z_7(0) = 0, z_8(0) = a_4, z_9(0) = 0, z_{10}(0) = a_5, z_{11}(0) = 0, z_{12}(0) = a_6, z_{13}(0) = 0, z_{14}(0) = a_7 \quad \ldots (21)$$

The above equations (20) are numerically solved by employing 4th order Runge-Kutta method subject to (21), where $a_1, a_2, a_3, a_4, a_5, a_6 \; and \; a_7$ a_1 are unknown values to be determined at the boundary condition λ=1 by usual Newton Raphson method. We have setup the convergence of atleast 10^{-6} in our calculations. The initial condition chosen to obtain 'a' values is [2, 2, 2, 2, 2, 2, 2]. Mat lab package has been used to get the relevant results.

4 Comprehensive discussion of the results

The resulting non-linear ordinary differential equations (11) to (15) in conjugation with (16) have been solved numerically through the shooting method concept and subsequently we analyzed the impact on components of temperature distribution, velocity and concentration profiles for couple stress fluid parameter (α)**,** suction-injection ratio (a), Reynolds number (Re), non dimensional thermophoresis parameter (Nt), Brownian motion parameter (Nb), radiation parameter (Rd) and Prandtl number (Pr) in detail and presented the outcomes through neat graphs. Skin friction coefficient, the rate of heat transfer and rate of mass transfer against specific fluid, geometric parameters are shown clearly in the form of tables.

The impact of couple stress fluid parameter (α) on velocity fields, temperature component, concentration profiles are displayed in Fig. 2. We noticed that as couple stress fluid parameter (α) augments the temperature and axial velocity also rises, but the concentration profiles diminished from lower plate (λ=0) to upper plate (λ=1) and also the radial velocity fields increase in the direction of the centre of the channel λ=0.5 then diminishes with the rising α. The impact of suction & injection ratio parameter 'a' on flow fields, heat, and mass transfer components are depicted in Fig. 3. we observed from that figure, that the axial velocity fields and concentration distribution are diminishing with augment of 'a', due to the fact that as 'a' increases suction velocity decreases, but the radial velocity and temperature escalate as λ moves from 0 to 1. The affect of Reynolds number (Re) on velocity fields, temperature components, and

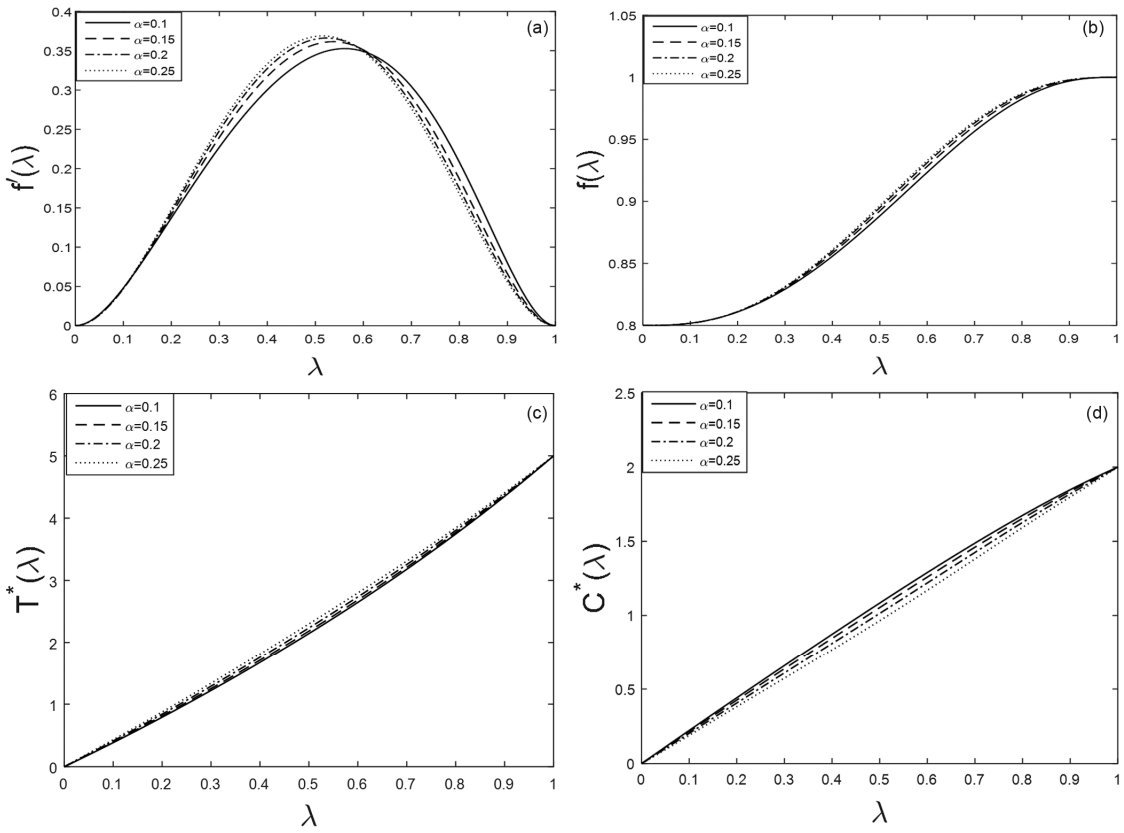

Fig. 2 — Influence of "α" on the (a) primary-velocity, (b) secondary-velocity, (c)the temperature, (d) the concentration, For wt=0.25; Re=4; Da=0.5; ξ=0.6325; Ec=0.2; Gr=17; Gm=17; Pr=0.5; Nt=0.37; Nb=0.2; Re=4; Sc=0.2; Sh=0.5; a=0.2; Rd=0.25.

concentration components are shown in Fig. 4. As Reynolds number increases, axial velocity profile, temperature and concentration components decrease because an increase in Reynolds number will increase the suction velocity, whereas radial velocity decreases up to λ=0.5 and subsequently it increases for other

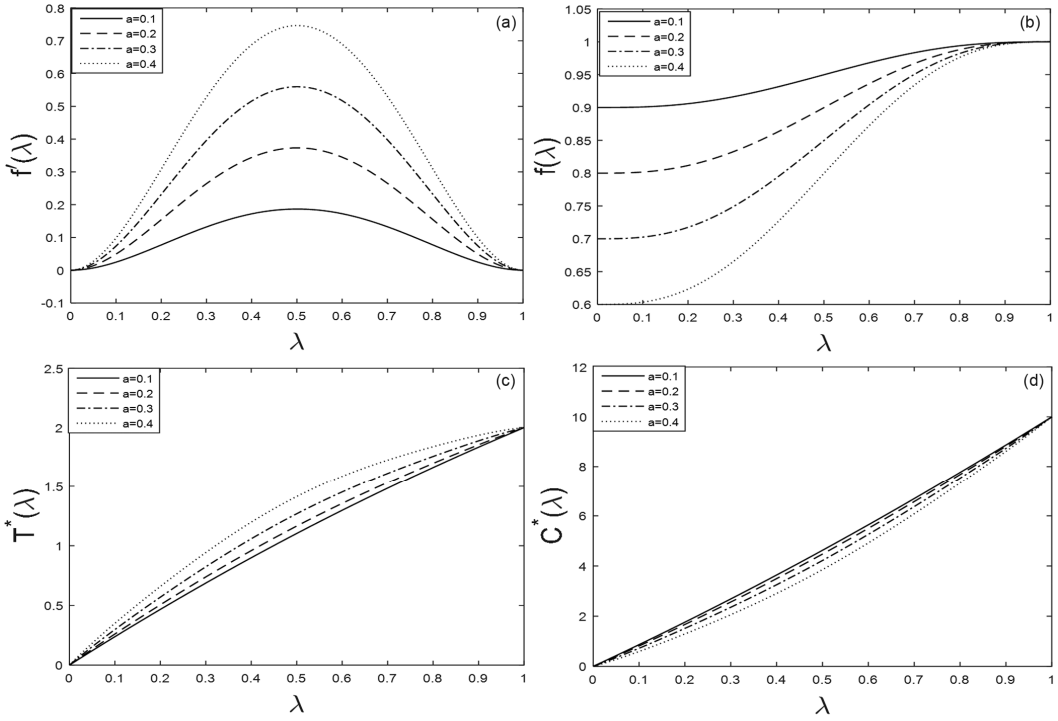

Fig. 3 — Influence of "a" on the (a) primary-velocity, (b) secondary-velocity, (c)the temperature, (d) the concentration, For wt=0.25; Re=0.5; Da=0.2; ξ=0.6325; Ec=0.5; Gr=5; Gm=5; α=0.5; Pr=0.4; Nt=0.2; Nb=0.4; Sc=0.2; Sh=0.1; Rd=0.25.

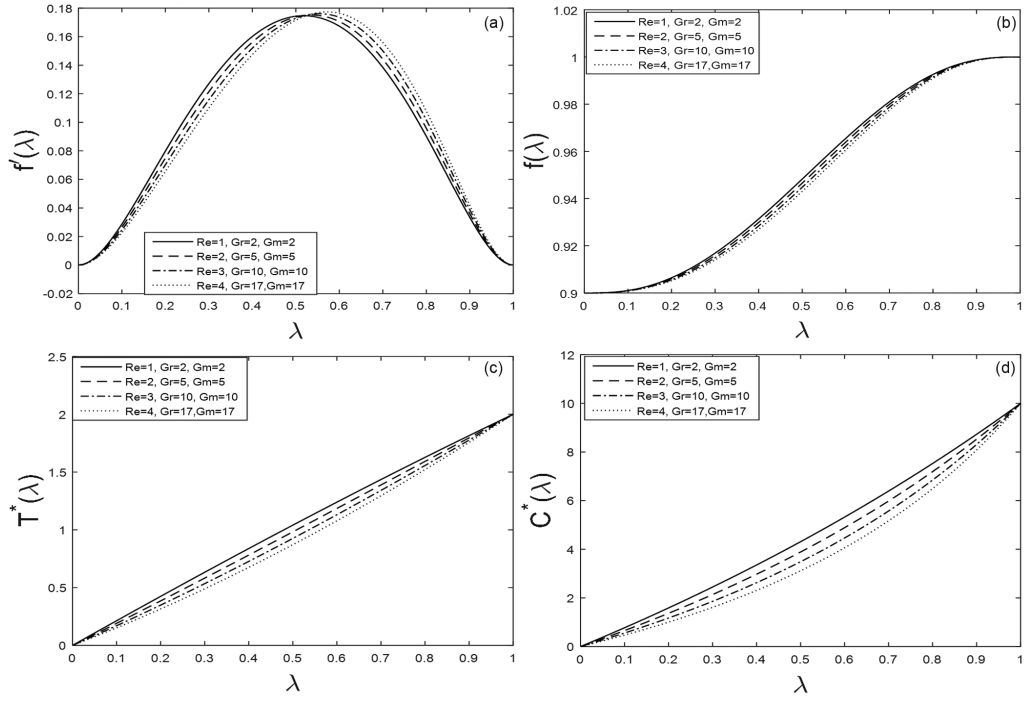

Fig. 4 — Impact of "Re, Gr and Gm" on (a) primary-velocity, (b) secondary-velocity, (c) the temperature, (d) the concentration For wt=0.1; Da=0.3; ξ=0.6325; Ec=0.5; α=0.1; Pr=0.5; Nt=0.2; Sc=0.5; Sh=0.1; a=0.1; Nb=0.4; Rd=0.5.

values of λ. Fig. 5 indicates the sway of Nt (thermophoresis parameter) on the temperature distribution and the concentration profiles. From the

Fig. 5, we observe that as Nt augments, the temperature distribution increases towards the λ=1 due to gradual growth in nanoparticle percentage. However the concentration fields decrease from bottom plate λ=0 to top plate λ=1. The significance of Brownian parameter (Nb) on temperature characteristics and the concentration characteristics are observed in Fig. 6. It is perceived that Nb is directly proportional to the temperature and concentration profiles. The impact of Rd (radiation parameter) on temperature and concentration distributions is shown in Fig. 7. It is examined that by enhancing Rd values the concentration distribution is also increasing, but the temperature profile decreases from the bottom plate (λ=0) to the top plate (λ=1) due

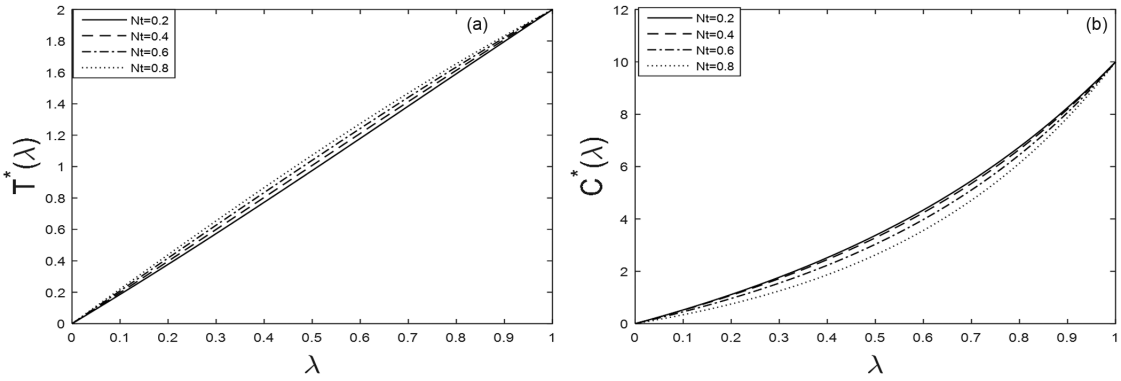

Fig. 5 — Impact of "Nt"on (a) the temperature (b) the concentration For wt=0.1; Re=3; Da=0.75; ξ=0.6325; Ec=0.5; Gr=10; Gm=10; α=0.1Rd=0.5; Pr=0.5; Nb=0.4; Sc=0.5; Sh=0.1; a=0.1.

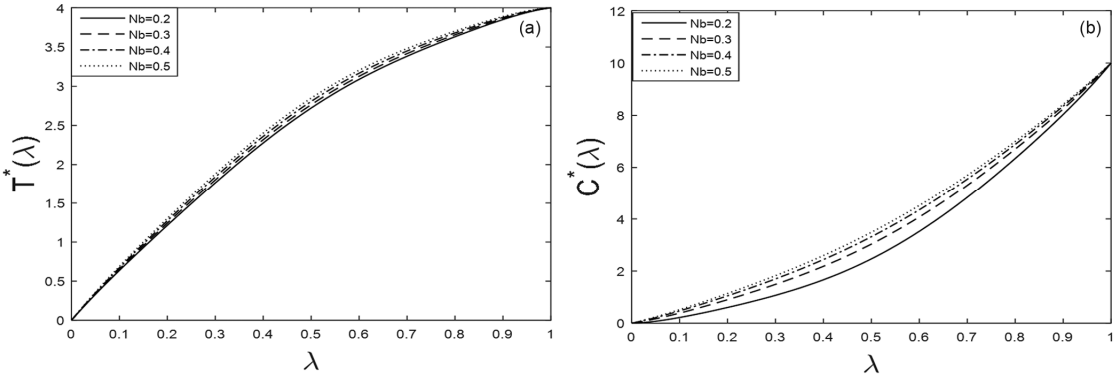

Fig. 6 — Impact of "Nb" on (a) the temperature, (b) the concentration For wt=0.25; Re=3; Da=0.2; ξ=0.6325; Gr=10; Ec=0.25; Sh=0.1; Gm=10; Rd=0.1; β_1=0.3; Sc=0.2; Nt=0.2; Pr=0.25; a=0.3;α=0.5

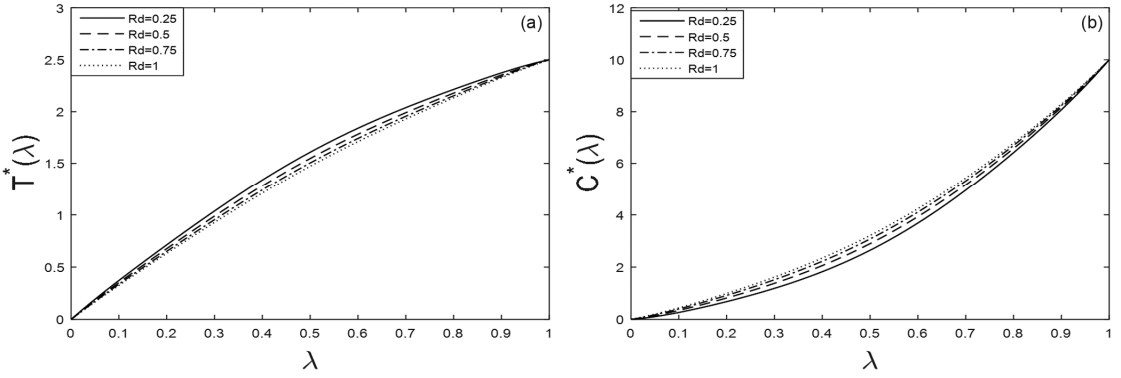

Fig. 7 — Impact of "Rd" on (a) temperature, (b) concentration For wt=0.25; Da=0.2; ξ=0.6325; Ec=0.4; Gr=5; Gm=5; α=0.5;Pr=0.4; Nt=0.4; Sc=0.4; Sh=0.1; a=0.2; Nb=0.4; Re=2.

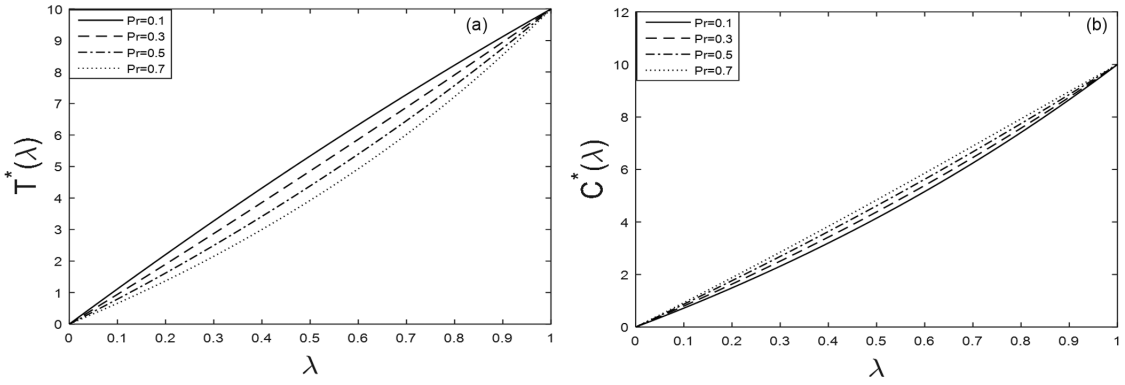

Fig. 8 — Impact of "Pr" on (a) temperature, (b) concentration For wt=0.25; Da=0.2; ξ=0.6325; Ec=0.1; Gr=10; Gm=10; α=0.5; Rd=0.25; Nt=0.4; Sc=0.2; Sh=0.1; a=0.1; Nb=0.2; Re=3.

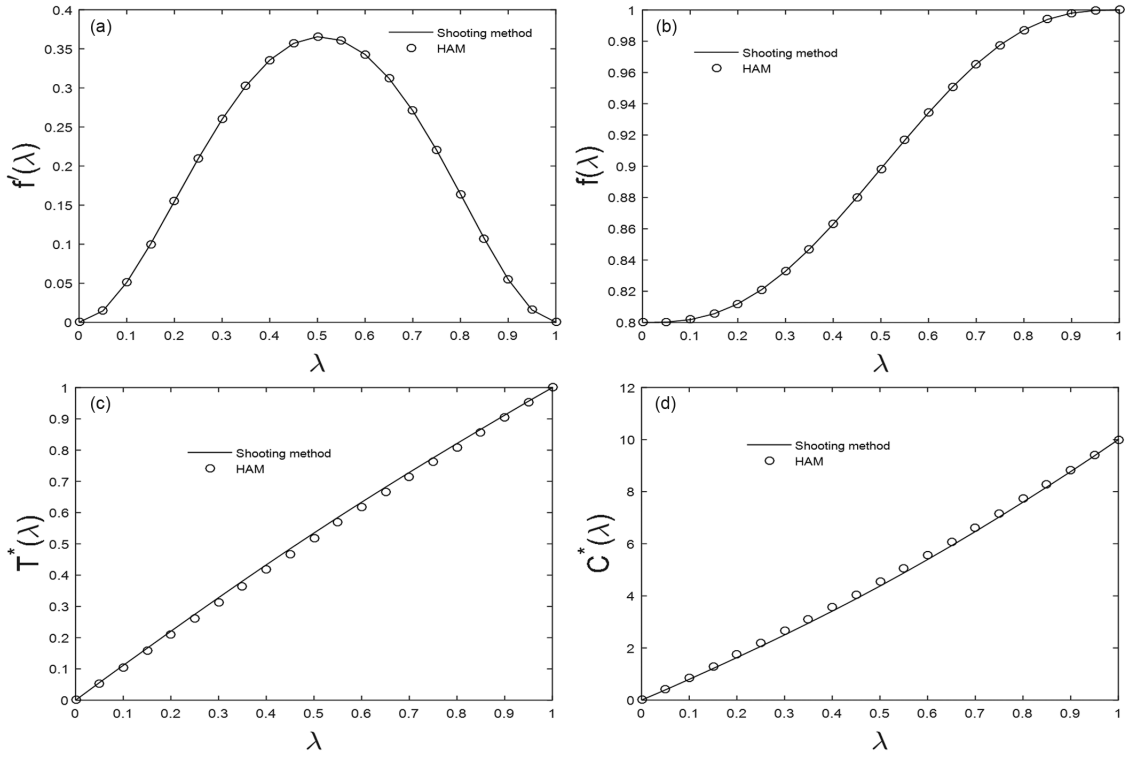

Fig. 9 — Comparison of Shooting method with Homotopy analysis method for on (a) primary velocity, (b) secondary velocity, (c) the temperature, (d) the concentration at wt=0.25; Re=3; Da=0.2; ξ=0.6325; Ec=0.1; Gr=10; Gm=10; Rd=0.25; α=0.5; Nb=0.4; Nt=0.2; Sc=0.2; Sh=0.1; a=0.1.

to the fact that the radiation is inversely proportional to thermal conductivity and mean absorption rate. The impact of Pr (Prandtl number) on temperature and concentration distribution can be seen in Fig. 8. From this figure, as long as Pr value increases temperature decreases because with the increase in prandtl number there is decreases in thermal diffusivity, whereas concentration increases from non-dimensional height λ=0 to λ=1. In Fig. 9 we presented a comparision of the results obtained from the shooting method with the Homotopy analysis method and found that, both the results are in good agreement with each other. The same can be seen in Table 1 & 2. In addition to this we compared the results obtained by us using shooting method and Homotopy analysis method with the results existing in literature[13]. The comparison is shown in the form of Table 3 and are found to be in good agreement. This validates our approach.

Table 4 shows the numerical outcomes of skin-friction coefficient at lower and at the upper plates for

Table 1 — Axial, Radial velocities Results Comparison with Shooting method and HAM Method

	Axial Velocity		Radial Velocity	
λ	Shooting Method	HAM		Shooting Method
0	0	0	0.8	0.8
0.1	0.51130	0.051130	0.801827	0.801826
0.2	0.154874	0.154875	0.811943	0.811942
0.3	0.259852	0.259852	0.83282	0.83282
0.4	0.335668	0.335668	0.862926	0.862926
0.5	0.365516	0.365515	0.898411	0.8984106
0.6	0.342802	0.342804	0.934267	0.934267
0.7	0.270696	0.270695	0.965312	0.965312
0.8	0.164181	0.1641817	0.987241	0.987241
0.9	0.0549627	0.0549627	0.998031	0.998030
1.0	0	$9.76996*10^{-15}$	1	0.999999

Table 2 — Temperature and concentration results Comparison with Shooting method and HAM Method

	Temperature		Concentration	
λ	Shooting Method	HAM	Shooting Method	HAM
0	0	0	0	0
0.1	0.105155	0.105155	0.859326	0.859326
0.2	0.209228	0.209228	0.74618	1.74617
0.3	0.313564	0.313563	2.64771	2.64771
0.4	0.417104	0.417104	3.57544	3.57543
0.5	0.518543	0.518543	4.54386	4.54386
0.6	0.61726	0.61726	5.56106	5.56106
0.7	0.713696	0.713695	6.62456	6.62456
0.8	0.809208	0.809207	7.72244	7.722436
0.9	0.905125	0.905124	8.8425	8.842497
1.0	1	1	10	10

Table 3 — Comparison of current work with already published work for Newtonian fluid with suction case Terrill & Shrestha[13].

$a(\alpha_2)$	Re	Skin-friction at λ=0			Skin-friction at λ=1		
		Terril & Shresta[13]	Series Solution	Present	Terril & Shresta[13]	Series Solution	Present
1.943	72.826	126.2	128.1	126.2	-134.6	-137.1	-134.7
1.916	77.476	128.8	130.7	132.1	-142.0	-144.4	-146.1
1.931	77.387	132.0	133.7	132.3	-143.0	-145.2	-143.2
1.905	79.968	131.0	132.5	130.9	-146.3	-148.4	-146.2

Table 4 — Skin-friction at the lower and the upper plates for ξ = 0.6325, Pr=0.5, Nb =0.4, Sc=0.5, Sh=0.1, Nt =0.2 , Rd=0.5.

Re, Gr, Gm	α	A	Da	Wt	Ec	Skin friction at λ=0	Skin friction at λ=1
1,3,3	0.1	0.1	0.3	0.1	0.2	1.0489	-1.2684
2,5,5						0.9562	-1.3975
3,10,10						0.8746	-1.5417
4,17,17						0.8030	-1.7020
	0.1					1.0489	-1.2684
	0.2					2.1541	-2.3876
	0.3					3.9521	-4.1913
	0.4					6.4615	-6.7042
		0.1				1.0484	-1.2689
		0.2				2.1018	-2.5244
		0.3				3.1605	-3.7664
		0.4				4.2247	-4.9948
			0.3			1.0484	-1.2689
			0.5			1.0521	-1.2723
			0.7			1.0558	-1.2756
			0.9			1.0595	-1.2790

(*Contd.*)

Table 4 — Skin-friction at the lower and the upper plates for ξ = 0.6325, Pr=0.5, Nb =0.4, Sc=0.5, Sh=0.1, Nt =0.2 , Rd=0.5.

(*Contd.*)

Re, Gr, Gm	α	A	Da	Wt	Ec	Skin friction at λ=0	Skin friction at λ=1
				0.1		1.0484	-1.2689
				0.2		1.0341	-1.2481
				0.3		1.0104	-1.2137
				0.4		0.9773	-1.1662
					0.5	1.0484	-1.2689
					0.6	1.0482	-1.2691
					0.7	1.0481	-1.2693
					0.8	1.0479	-1.2694

Table 5 — Nusselt number and Sherwood number at the lower and upper plates

Ec	α	Rd	Sc	Nt	Nb	Nusselt number at λ=0	Nusselt number at λ=1	Sher wood number at λ=0	Sher wood number at λ=1
0.1						-13.4936	-11.5057	-9.1653	-10.8820
0.2						-6.9699	-5.5159	-8.9895	-11.0746
0.3						-4.7954	-3.5193	-8.8136	-11.2672
0.4						-3.7081	-2.5210	-8.6377	-11.4598
	0.1					-13.4936	-11.5057	-9.1653	-10.8820
	0.3					-13.5251	-11.4757	-9.1526	-10.8946
	0.5					-13.5867	-11.4157	-9.1282	-10.9190
	0.7					-13.6790	-11.3256	-9.0916	-10.9557
		0.25				-13.4936	-11.5057	-9.1653	-10.8820
		0.5				-15.9911	-14.0034	-9.2314	-10.8154
		0.75				-18.4894	-16.5017	-9.2785	-10.7676
		1				-20.9880	-19.0005	-9.3136	-10.7317
			0.2			-13.4936	-11.5057	-9.1653	-10.8820
			0.4			-13.4776	-11.4920	-8.7477	-11.3868
			0.6			-13.4616	-11.4784	-8.3432	-11.9067
			0.8			-13.4457	-11.4649	-7.9517	-12.4415
				0.1		-13.4936	-11.5057	-9.1653	-10.8820
				0.3		-14.5275	-10.6008	-7.1578	-12.7954
				0.5		-15.6111	-9.7458	-3.4186	-16.0821
				0.7		-16.7438	-8.9399	2.1703	-20.6240
					0.2	-13.4936	-11.5057	-9.1653	-10.8820
					0.4	-14.5102	-10.5883	-9.1606	-10.8665
					0.6	-15.5742	-9.7228	-9.1527	-10.8544
					0.8	-16.6848	-8.9084	-9.1441	-10.8432

ξ = 0.6325, Rd=0.5, Pr=0.5, Nb =0.4, Nt =0.2, Sc=0.5, Sh=0.1 by increasing Re, α, a, Da, Ga, Ec. It is observed that the Skin- friction coefficient values at lower plate are increasing with α, a, Da where as it decreases with Re, Ga and Ec. At the top plate (λ=1) skin friction is increased for Re, a, Da and Ec where as decreasing for α, Ga.

Table 5 indicates the numerical outcomes of rate of heat and mass transfers at the lower and the upper plates for Ga=0.25, Re=0.5, Da=0.2, ξ = 0.6325, Gr=5, Gm=5, Pr=0.4, Sh=0.1, a=0.1. It is noticed that as Ec, α, Rd, Sc, Nt and Nb increases, the heat transfer rate at the lower plate also enhances for increasing α, Rd, Nt and Nb, But decreases for increasing Ec and SC. For the upper plate, the heat transfer rate is increasing for higher Rd whereas it diminishes for higher Ec, α, Sc, Nt, and Nb. The Mass transfer rate at the lower plate uptrend with higher Rd whereas decreases for increasing Ec, α, Sc, Nt, and Nb. The Mass transfer rate through the upper plate enhances with an increase in Ec, α, Sc and Nt while decreasing with increasing Rd & Nb.

5 Conclusions

In this current work, the energy and concentration characteristics of natural convective couple stress nanofluid flow confined to two porous horizontal parallel plates with thermophoretic diffusion & the Brownian movement effects are considered. The outcomes are analyzed for the dimensionless velocity profile, energy and concentration characteristics. Also, the skin friction coefficient, the

Nusselt number & the Sherwood number with regarding to different fluid parameters and also geometric parameters are investigated. Important results can be summarized as

i. The temperature distribution of the fluid is augmented with Thermophoretic diffusion and Brownian motion parameters where as exhibiting the opposite trend for large values of radiation parameter.
ii. The concentration distribution of the fluid increased with the radiation parameter while opposite behaviour is observed with couple stress fluid parameter.
iii. The temperature profiles are increased for suction/injection ratio, but it is having reverse trend in case of Reynolds number.
iv. The temperature and concentration distributions behave in a similar fashion for both Prandtl number and radiation parameter.
v. The coefficient of skin-friction through the upper plate (λ=1) is enhanced with the frequency parameter (ωt).
vi. The method adopted as well as the results obtained have been validated and are found to be agreeing well with the existing literature.

Acknowledgments

The authors would like to thank Dr Srinivas Jangili, NIT Warangal for his valuable suggestions in the preparation of the manuscript.

Nomenclature

C concentration
$C_1e^{i\omega t}$ lower plate concentration
$C_2e^{i\omega t}$ upper plate concentration
T^* non dimensional temperature, $\frac{T-T_1e^{i\omega t}}{(T_2-T_1)e^{i\omega t}}$
C^* Dimensionless concentration, $\frac{C-C_1e^{i\omega t}}{(C_2-C_1)e^{i\omega t}}$
η_A mass transfer rate
h distance between parallel plates
p fluid pressure
Ec Eckert number, $\frac{\mu V_2}{\rho hc(T_2-T_1)}$
Da Darcy parameter
Re Reynolds number, $\frac{\rho V_2 h}{\mu}$
K Thermal conductivity
K_1 permeability parameter
D Molecular diffusion coefficient
D_B Brownian diffusion coefficent
Sh Sherwood number, $\frac{\eta_A}{h\vartheta(C_2-C_1)}$
Pr Prandtl number, $\frac{\mu C}{K}$
Gm solutal Grashof number, $\frac{\rho g\beta_C(C_2-C_1)h^2}{\mu V_2}$
Gr thermal Grashof number, $\frac{\rho g\beta_T(T_2-T_1)h^2}{\mu V_2}$
Rd Radiation parameter, $\frac{16\sigma T_1^3}{3KK_3}$
Nb Non dimensional Brownian parameter, $\frac{D_B(C_2-C_1)(\rho C)_P}{\mu V_2(\rho C)_f}$
Nt Non dimensional thermophoresis parameter, $\frac{D_T(T_2-T_1)(\rho C)_P}{\vartheta T_1(\rho C)_f}$
Sc Schmidt number, $\frac{\vartheta}{D_1}$
a Injection/Suction ratio
T Temperature
t Time
u,v X,Y-direction velocity components respectively

Greek Letters

λ y- coordinate non –dimensional, $\frac{y}{h}$
β_T Thermal expansion coefficients
β_C Solutal expansion coefficients
ξ axial length variable, $\left(\frac{U_0}{av_2}-\frac{x}{h}\right)$
Ψ frequency parameter, ωt
ρ Fluid density
α Couple stress fluid parameter, $\sqrt{\frac{\eta}{\mu h^2}}$

References

1 Stokes V K, *Phys Fluids*, 9 (1966) 1709.
2 Stokes V K, *In Theories of Fluids with Microstructure Springer*, Berlin, Heidelberg (1984) 34.
3 Srinivasacharya D, Srinivasacharyulu N & Odelu O, *Int J Appl Math*, 41 (2011) 10.
4 Devakar M & Iyengar T KV, *Nonlinear Anal Model Control*, 15 (2010) 29.
5 Srinivasacharya D & Kaladhar K, *Commun Nonlinear Sci Numer Simul,* 17 (2012) 2447.
6 Aksoy Y, *Int J Therm Sci,* 107 (2016) 1.
7 Ojjela O & Kumar N N , *Arab J Sci Eng*, 41(5 (2016) 1941.
8 Hayat T , Sajjad R, Alsaedi A, Muhammad T & Ellahi R , *Results Phys*, 7 (2017) 553.
9 Parvazinia M, Nassehi V, Wakeman R J & Ghoreishy M H R, *Trans porous Media*, 63 (2006) 71.
10 Ojjela O & Kumar N N, *Proceedings of the International Conference on Mechanics, Fluids, Heat, Elasticity, and Electromagnetic Fields*, (2013) 161.
11 Idowu A S & Olabode J O, *IOSR J Math*, 10 (2014) 47.

12 Attia H A, Abbas W, Abdeen M A & Said A A, *Sadhana,* 40 (2015) 183.
13 Terrill R M & Shrestha G M, *Appl Sci Res Section A*, 15 (1966) 440.
14 Das, S, *Indian J Pure Appl Phys,* 54 (2016) 517.
15 Nakamura H, Asako Y & Naitou T, *Numer Heat Transf Part A Appl*, 5 (1982) 95.
16 Narahari M *MACMESE'09 Proceedings of the 11th WSEAS Int Conference Mathematical Comput Methods Sci Eng*, 73 (2009).
17 Narahari M & Dutta B K, *Acta Tech*, 56 (2011) 103.
18 Jha B K & Ajibade A O, *Commun Nonlinear Sci Numer Simul*, 17 (2012) 1576.
19 Jha B K & Aina B, *Alex Eng J*, 55 (2016) 2087.
20 Alagoa K D, Tay G & Abbey T M, *Astrophys Space Sci*, 260 (1998) 455.
21 Kumar M S, Sandeep N & Kumar B R, *Glob J Pure Appl Math*, 12 (2016).
22 Dogonchi A S, Divsalar K & Ganji D D, *Comput Methods Appl Mech Eng*, 310 (2016) 58.
23 Hassan A R, Gbadeyan J A & Salawu S O, *In Int Conference on Appl Math Model. Comput Sci*, *Springer Cham,* (2017) 183.
24 Reddy P S, Chamkha A J & Al-Mudhaf A, *Adv Powder Technol*, 28 (2017) 1008.
25 Sandhya A, Reddy G & Deekshitulu G V S R, *J Pure Appl Phys*, 58 (2020) 548.
26 Brown R, *Philos l Mag*, 4 (1828) 161.
27 Buongiorno J, *J Heat Transf*, 128 (2006) 240.
28 Guha A & Samanta S, *Int J Heat Mass Transf,* 68 (2014) 42.
29 Mahmoodi M & Kandelousi S, *J Mol Liq,* 211 (2015) 15.
30 Hayat T, Muhammad T, Qayyum A, Alsaedi A & Mustafa M , *J Mol Liq*, 213 (2016) 179.
31 Sheikholeslami M, Rashidi M M, Al Saad D M, Firouzi F, Rokni H B & Domairry G, *J King Saud Uni Sci*, 28 (2016) 380.
32 Reddy J R, Sugunamma V & Sandeep N, *Alex Eng J*, 57 (2018) 2465.